Available online at www.sciencedirect.com
SCIENCE DIRECT®
Journal of Power Sources 119–121 (2003) 64–68
JOURNAL OF POWER SOURCES
www.elsevier.com/locate/jpowsour

Alternative anode materials for lithium-ion batteries: a study of Ag_3Sb

J.T. Vaughey[a,*], L. Fransson[b], H.A. Swinger[a], K. Edström[b], M.M. Thackeray[a]

[a]*Electrochemical Technology Program, Chemical Technology Division, Argonne National Laboratory, Argonne, IL 60439, USA*
[b]*Department of Materials Chemistry, Ångstrom Laboratory, Uppsala University, S-751-21 Uppsala, Sweden*

Abstract

Silver antimonide, Ag_3Sb, in which silver and antimony are both electrochemically active toward lithium, has been studied as an anode for lithium-ion batteries. The rate of capacity fade on cycling was monitored as a function of the voltage window, which has provided further information about the causes of capacity fade in intermetallic electrode systems. From the voltage profiles, and by comparison with the behavior of SnSb, InSb and Cu_2Sb electrodes, the electrochemical reaction of Li/Ag_3Sb cells was determined to take place in several discrete stages: first, by a displacement reaction in which lithium replaces Ag in the Ag_3Sb structure in a two-step process between 0.9 and 0.7 V to form Li_3Sb via Li_2AgSb; and second, by reaction of lithium with the extruded silver between 0.2 and 0.0 V to form Li_xAg compounds ($1 \leq x \leq 4$). The rate of capacity fade that occurs when cells are cycled between 1.2 and 0.0 V was significantly reduced by limiting the reaction to either: (1) the low voltage region (0.7–0.0 V), which provided a stable capacity of ~300 mAh/g; or (2) to a wider operating window (1.2–0.1 V, 250 mAh/g), in which the formation of Li_xAg phases was suppressed.

Keywords: Lithium-ion batteries; Intermetallic electrodes; Anodes; Silver antimony

1. Introduction

Negative electrodes (anodes) for lithium-ion batteries must possess a diverse range of structural and electrochemical properties, which make the rational design of anode materials a difficult assignment. Required properties include a low potential versus metallic lithium, a specific capacity greater than 300 mAh/g, high cycling efficiency, low irreversible capacity, high levels of safety, and low cost. In lithium-ion cells, the anode material of choice is graphite. Intrinsically, graphite has many of the desired characteristics while other properties, such as safety, can be engineered into the system by introducing electronic voltage controls to prevent cells from being overcharged. However, avenues for new materials' advances remain open because higher levels of safety, and higher specific and volumetric capacity than those offered by graphite are still desirable. In the past, alternative electrodes to graphite have been proposed, for example, those based on: (1) elemental aluminum, silicon or tin [1]; (2) composite structures formed in situ by electrochemical reduction of metal oxides [2,3]; and (3) host structures in which there is a strong structural relationship between the parent structure and its lithiated product, as observed for Cu_6Sn_5 [4,5] and MnSb [6], and particularly those host structures that maintain a stable face-centered-cubic (fcc) array during reaction with lithium, such as SnSb [7], InSb [8] and Cu_2Sb [9].

Most of the alternative anode systems studied to date have addressed materials issues with varying degrees of success, although no one system has yet been able to satisfy all of the performance requirements. Among the more promising alternatives to carbon electrodes are intermetallic compounds. They have attractive electrochemical properties including a high volumetric capacity and a higher (safer) operating potential compared to lithiated graphite. On the other hand, as presently configured, they tend to show a higher irreversible capacity than graphite and a higher fade rate on subsequent cycles. Several explanations for this behavior have been given, such as the loss of electronic contact between electrode particles, solid–electrolyte–interphase (SEI) formation, the formation of oxide passivation layers during processing, and binder degradation [7,10].

One of the major requirements of lithium-ion batteries is that the electrolyte and electrode binder remain stable over the full operating potentials of the electrodes. Most film-forming electrolytes, usually containing ethylene carbonate, have been optimized for use with graphite anodes. During the electrochemical reaction with lithium at low potentials, metals can be displaced from the parent structures of intermetallic or metal oxide electrodes, such as Cu_2Sb and CoO, and extruded to the surface of the electrode particles in very

* Corresponding author. Tel.: +1-630-252-8885; fax: +1-630-252-4176.
E-mail address: vaughey@cmt.anl.gov (J.T. Vaughey).

0378-7753/03/$ – see front matter
doi:10.1016/S0378-7753(03)00126-5

finely divided form; the extruded metals (Cu and Co, respectively) can be expected to react with the electrolyte and binder. Chemical analysis and film characterization have shown that in such instances, particularly for lithiated CoO electrodes, the SEI layer is similar to the one formed on lithiated graphites [11,12]. Studies of Cu_2Sb electrodes in Li/Cu_2Sb cells have shown that the extruded copper can be reinserted into the Sb array with remarkable efficiency during charging, despite the presumed presence of a SEI layer on the copper particles [9].

In this study, the electrochemical behavior of Li/Ag_3Sb cells has been examined when cells were cycled between three different voltage limits, 1.2–0.0, 0.7–0.0 and 1.2–0.1 V. The voltage profiles are discussed in terms of structural changes that are expected to occur in lithiated Ag_3Sb electrodes according to the Li–Ag–Sb phase diagram; the data provide a further understanding of the factors that control the electrochemical reversibility of intermetallic electrodes in lithium cells.

2. Experimental

Silver antimonide, Ag_3Sb, was prepared by reacting stoichiometric amounts of metallic silver (Aldrich, 99.99%) and antimony (Aldrich, 99.9%) at 800 °C under argon for 8 h. The product was isolated as an ingot and ground with 5 wt.% carbon to a fine powder by ball milling the sample for 1 h. The carbon was added to prevent the material from sticking to the ball mill container walls. Powder X-ray diffraction data, collected on a Siemens D5000 powder diffractometer with Cu Kα between 10 and 80° 2θ at a scan rate of 0.6° 2θ/min, showed that the Ag_3Sb sample was single phase.

Electrodes were fabricated from an intimate mixture of the 80% Ag_3Sb powder with an approximately 10 μm average particle size, 10% polyvinylidene difluoride polymer binder (Kynar) and 10% acetylene black in 1-methyl-2-pyrrolidinone. The electrode mixture was dried at 75 °C for 10 h, and dried again under vacuum at 70 °C for 12 h. The electrodes were evaluated at room temperature in coin-type cells (size 2032, Hohsen) with a lithium foil counter electrode (FMC Corp., Lithium Div.), Celgard separator (Hoechst-Celanese) and a 1 M $LiPF_6$ in EC/DEC electrolyte. Cells were constructed inside a dryroom (<200 ppm, H_2O) and cycled on a Maccor Series 2000 tester under galvanostatic mode at 0.16 mA/cm^2. Current interruptions were carried out every 30 min in order to monitor cell impedance.

3. Results and discussion

Metal antimonides, M_xSb, particularly those with a face-centered-cubic Sb array (sometimes slightly distorted from ideal packing), have recently received considerable interest as possible negative electrode materials for lithium-ion batteries. Notable examples of these compounds are SnSb (rock salt-type structure) [7], InSb (zinc blende-type structure) [8] and Cu_2Sb [9]. During the electrochemical reactions of these intermetallic compounds, lithium is inserted into the M_xSb structure with the concomitant expulsion of the metal, M, from the structure to yield Li_3Sb without disrupting the fcc Sb host array. Further reaction of lithium is sometimes possible, as it is with the extruded Sn and In from SnSb and InSb electrodes, respectively, but not with the extruded Cu from Cu_2Sb. If the reaction with the M_xSb electrodes is limited to the lithium insertion/metal extrusion process, then excellent rechargeability can be obtained, as was observed with Cu_2Sb electrodes [9]. By contrast, if the extruded Sn and In from SnSb and InSb electrodes are allowed to react fully with lithium to yield $Li_{4.4}Sn$ and $Li_{4.3}In$ compounds, respectively, then the capacity of the Li/M_xSb cells declines rapidly. Cu_2Sb is a particularly attractive electrode material because the inserted lithium is more compatible with the size of the copper atoms than it is with metals, such as Sn and Sb, a feature that is believed to contribute to the excellent electrochemical behavior of Cu_2Sb. This study on Ag_3Sb was prompted because both copper and silver are group 1b elements with excellent electronic conductivity. However, unlike copper, silver can form several binary compounds with lithium, Li_xAg for ($1 \leq x \leq 4$), although most of these phases, besides LiAg, have not yet been characterized in detail [13]; in this paper, for the sake of simplicity, these compounds are referred to generally as Li_xAg with end members LiAg and Li_4Ag. Although a report on the electrochemical behavior of Li/Ag_3Sb cells, cycled between 2.5 and 0.0 V, has appeared recently, little information about the reaction processes that occur during discharge and charge, particularly from a structural viewpoint, were provided [14].

A schematic illustration of the Li–Ag–Sb phase diagram is shown in Fig. 1. The previously reported binary and ternary phases in this system that are of importance to this discussion are Ag_3Sb [15], Li_2AgSb [16], Li_3Sb [17], LiAg [18] and Li_4Ag [19]. If thermodynamic equilibrium was achieved at all states of charge and discharge, then the discharge of Li/Ag_3Sb cells would be defined by the following reaction sequence, for which the cumulative, theoretical specific capacities of the Ag_3Sb electrode are provided:

$$2Li + Ag_3Sb \rightarrow Li_2AgSb + 2Ag \quad (120\,mAh/g) \tag{1}$$

$$Li + Li_2AgSb \rightarrow Li_3Sb + Ag \quad (180\,mAh/g) \tag{2}$$

$$3Li + 3Ag \rightarrow 3LiAg \quad (360\,mAh/g) \tag{3}$$

$$9Li + 3LiAg \rightarrow 3Li_4Ag \quad (902\,mAh/g) \tag{4}$$

$$15Li + Ag_3Sb \rightarrow Li_3Sb + 3Li_4Ag \quad (902\,mAh/g) \tag{5}$$

During reactions (1) and (2), lithium is inserted into, and silver extruded from, the Ag_3Sb structure to initially form Li_2AgSb and thereafter Li_3Sb; during this process, the average composition of the Ag_3Sb electrode varies along the dashed line between Ag_3Sb and the Li apex of the

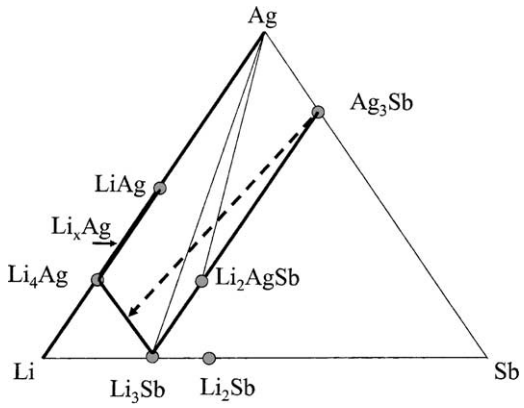

Fig. 1. A schematic illustration of the Li–Ag–Sb phase diagram showing the changes in composition of the components of a Ag_3Sb electrode during their reaction with lithium (arrowed directions). The dotted line represents the change in the overall composition of the electrode.

Li–Ag–Sb tie-triangle until the Ag–Li_3Sb tie-line is reached. Thereafter, lithium reacts with the extruded silver within a Li_3Sb matrix to form Li_xAg phases between LiAg and Li_4Ag until the overall composition of the electrode reaches the Li_4Ag–Li_3Sb tie-line (reactions (3) and (4)).

The electrochemical profiles of cells discharged and charged between 0.0 and 1.2, and 0.0 and 0.7 V are shown in Figs. 2 and 3, respectively. These cells delivered initial capacities that were typically 65–75% of the theoretical value, corresponding to the reaction of 10–11 Li per Ag_3Sb unit. Both Figs. 2 and 3 show that the cell impedance, as reflected by the magnitude of the voltage relaxation during the 30 s interrupts, is significantly larger during the initial discharge (“break-in”) reaction than on subsequent cycles, which is consistent with the behavior typical of intermetallic electrodes. The voltage profile of the second and subsequent discharge reactions in Fig. 2 shows a two-step process between 0.9 and 0.7 V, consistent with reactions (1) and

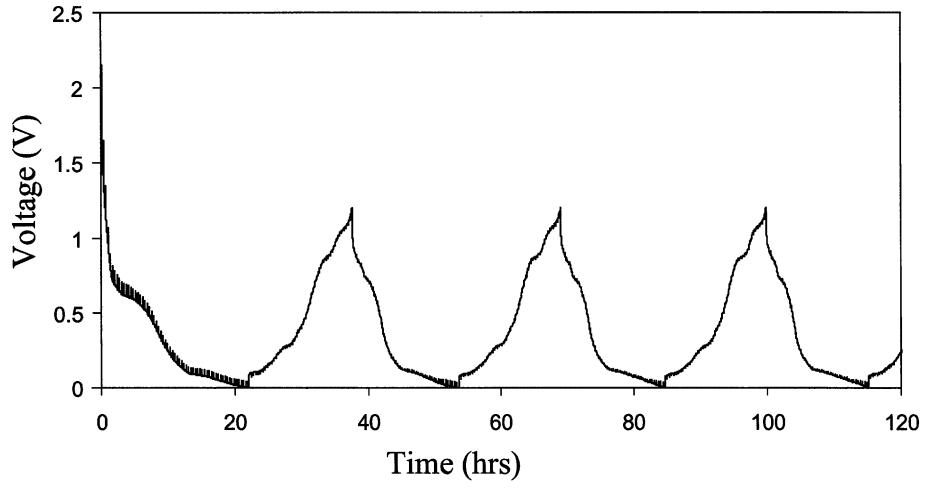

Fig. 2. The voltage profile of a Li/Ag_3Sb cell cycled between 1.2 and 0.0 V.

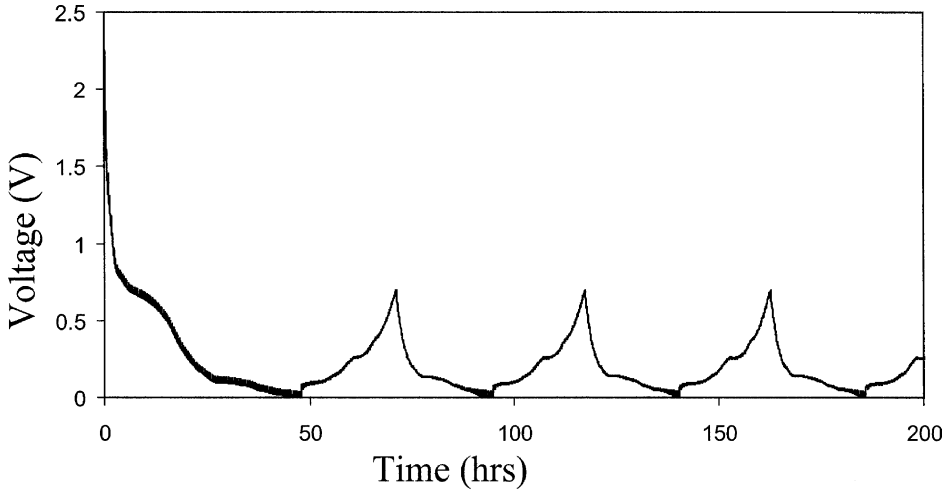

Fig. 3. The voltage profile of a Li/Ag_3Sb cell cycled between 0.7 and 0.0 V.

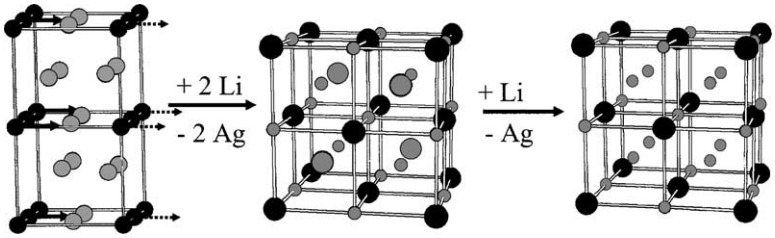

Fig. 4. The structures (from left to right) of Ag_3Sb, Li_2AgSb and Li_3Sb, showing the strong structural relationships between them and the displacement of 50% of the Sb atoms (arrowed) that is proposed to occur during the transition of Ag_3Sb to Li_2AgSb.

(2) above, in which Li_3Sb is formed from Ag_3Sb via a lithiated zinc blende, Li_2AgSb, intermediate structure. The structural relationships between Ag_3Sb, Li_2AgSb and Li_3Sb are shown in Fig. 4. The transition from Ag_3Sb to Li_2AgSb can occur if two lithium atoms are inserted into the Sb array with the simultaneous displacement of two Ag atoms from the structure and the concomitant internal displacement of one-half of the Sb atoms (shown by arrows in Fig. 4) into neighboring sites to generate the fcc Sb array in Li_2AgSb. During the transition from Li_2AgSb to Li_3Sb, the inserted lithium atoms replace the remaining Ag atoms in the structure without disturbing the fcc Sb array. Because these two transitions occur by displacement reactions in which small atoms (Li) replace relatively large ones (Ag), the unit cell volume actually decreases on lithium insertion by 5.8% (per Sb atom) during reaction (1) and by 0.2% (per Sb atom) during reaction (2). However, despite these small changes in unit cell volume, the orthorhombic a, b and c lattice parameters of Ag_3Sb (3.008, 4.828, and 5.214 Å) must change by +9.4, −31.8 and +26.2%, respectively, to yield the cubic lattice parameter of Li_2AgSb (6.583 Å). (Note, however, that there is only one Sb atom per Ag_3Sb unit cell, but four Sb atoms per Li_2AgSb unit cell, which requires a doubling of the orthorhombic a and b lattice parameters for these calculations.) Although Ag_3Sb, Li_2AgSb and Li_3Sb represent thermodynamically stable phases in the Li–Ag–Sb system, it is expected that in situ X-ray diffraction data, which are not yet available, will show solid–solution behavior between isostructural Li_2AgSb and Li_3Sb, as was observed in Cu_2Sb electrodes that showed solid solution behavior between Li_2CuSb and Li_3Sb [9].

When cells were cycled in the low-voltage range 0.7–0.0 V (Fig. 3), the predominant reaction occurs at approximately 0.15 V, which is attributed to the formation of LiAg. Two relatively minor processes occur between 0.1 and 0.0 V; they are attributed to the formation of Li_xAg phases between $x = 1$ and 4.

The capacity fade of Ag_3Sb electrodes when cycled in cells between 1.2 and 0.0, 1.2 and 0.1, and 0.7 and 0.0 V, is shown in Fig. 5. When cycled over the full compositional range, the capacity fade is relatively fast (Fig. 5a). This capacity fade is attributed to volumetric changes that are most severe when the electrodes are fully lithiated, which can lead to a break-up of the surrounding Li_3Sb matrix, electronic isolation of the particles, and the consequent trapping of lithium in heavily lithiated Li_xAg silver particles. This electronic isolation not only limits the removal of lithium from the silver particles, but also reduces the amount of silver that can be reintroduced into the fcc Sb array during charge. By contrast, when Ag_3Sb electrodes are cycled between 1.2 and 0.1 V, when the electrode is restricted to the composition LiAg at the end of discharge, then a considerable improvement in cycling stability is obtained with the electrodes delivering a steady capacity of ∼250 mAh/g (Fig. 5b). This observation is important because it demonstrates that, provided the lithiated silver particles remain closely connected to the Li_3Sb particles from which the extruded Ag was derived, the electrode can

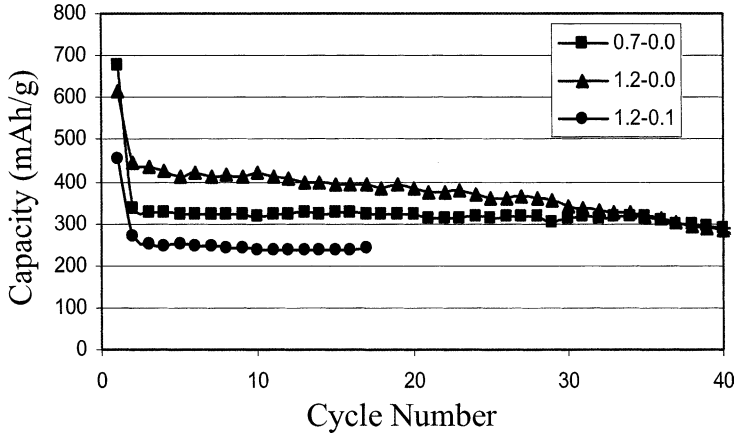

Fig. 5. Capacity vs. cycle number plots for Li/Ag_3Sb cells when discharged and charged over the voltage ranges: (a) 1.2–0.0 V; (b) 1.2–0.1 V; (c) 0.7–0.0 V.

cycle with good efficiency. Similar capacities and cycling efficiency have been obtained from InSb electrodes that were restricted to an end composition, $Li_3Sb + LiIn$, at the end of discharge, i.e. without allowing Li_xIn phases ($0 < x < 4.3$) to form [8,20]. Excellent cycling stability can be expected if the electrochemical reaction of Li/Ag_3Sb cells is restricted solely to the lithium insertion/silver extrusion process by limiting the cell voltage to ~0.5 V, but in this case the theoretical capacity of the electrode, defined by the reaction of three Li per Ag_3Sb unit, is only 180 mAh/g.

When Ag_3Sb electrodes are cycled in the low-voltage region (0.7–0.0 V), then a rechargeable capacity of ~300 mAh/g can be achieved (Fig. 5c). In this case, a Li_xAg electrode cycles within a composite Li_xAg/Li_3Sb matrix, in much the same way that a composite Li_xSn/Li_2O electrode, derived from amorphous SnO, operates [2,3]. It is believed that on reduction of Ag_3Sb and SnO electrodes, the Li_3Sb and Li_2O matrices function as stable ionically conducting ''blankets'', equivalent to the SEI layer on lithiated graphite electrodes, to protect the electrochemically active Li_xAg and Li_xSn components, thereby enhancing the reversibility and cycle life of these electrodes. However, in both examples, the Ag_3Sb and SnO electrodes suffer from large irreversible capacity losses on the initial cycle because much of the initial lithium remains inactive in the supporting Li_3Sb and Li_2O matrices, respectively.

4. Conclusions

The reversibility of Ag_3Sb electrodes in lithium cells has been investigated. The data are consistent with the behavior of other intermetallic electrodes, such as SnSb, InSb, Cu_2Sb that operate by lithium insertion/metal extrusion reactions. Although Li/Ag_3Sb cells lose capacity rapidly if the Ag_3Sb electrodes cycled over a wide compositional range (1.2–0.0 V), an improvement in cycling stability can be achieved either by restricting the reaction to a lithium insertion/silver displacement process and the lithiation of extruded silver to the composition LiAg (1.2–0.1 V), or by operating the cell over a narrower voltage range (0.7–0.0 V) in which silver is lithiated over to form Li_xAg phases ($0 < x < 4$) within a stable lithium-ion conducting Li_3Sb matrix.

Acknowledgements

Financial support from the Office of Basic Energy Sciences and from the Office of Advanced Automotive Technologies of the US Department of Energy, and from the Foundation for Environmental Strategic Research (MISTRA), the Nordic Energy Research Program (NERP), and the Swedish research council (VR) is gratefully acknowledged.

References

[1] R.A. Huggins, in: J.O. Besenhard (Ed.), Handbook of Battery Materials, vol. 1, Part III, Wiley-VCH, Wienheim, Germany, 1999, p. 359.
[2] Y. Idota, T. Kubota, A. Matsufuji, Y. Maekawa, T. Miyasaka, Science 276 (1997) 570.
[3] I.A. Courtney, J.R. Dahn, J. Electrochem. Soc. 144 (1997) 2045.
[4] K.D. Kepler, J.T. Vaughey, M.M. Thackeray, Electrochem. Solid State Lett. 2 (1999) 307.
[5] D. Larcher, L.Y. Beaulieu, D.D. MacNiel, J.R. Dahn, J. Electrochem. Soc. 147 (2000) 1658.
[6] L.M.L. Fransson, J.T. Vaughey, K. Edström, M.M. Thackeray, J. Electrochem. Soc. 150 (2003) A36.
[7] I. Rom, M. Wachtler, I. Papst, M. Schmied, J.O. Besenhard, F. Hofer, M. Winter, Solid State Ionics 143 (2001) 329.
[8] C.S. Johnson, J.T. Vaughey, M.M. Thackeray, T. Sarakonsri, S.A. Hackney, L.M.L. Fransson, K. Edström, J.O. Thomas, Electrochem. Commun. 2 (2000) 595.
[9] L.M.L. Fransson, J.T. Vaughey, R. Benedek, K. Edstrom, J.O. Thomas, M.M. Thackeray, Electrochem. Commun. 3 (2001) 317.
[10] M. Wachtler, J.O. Besenhard, M. Winter, J. Power Sources 94 (2001) 189.
[11] P. Poizot, S. Laurelle, S. Grugeon, L. Du Pont, J.-M. Tarascon, Nature 407 (2000) 496.
[12] S. Laruelle, S. Grugeon, P. Poizot, M. Dolle, L. Du Pont, J.M. Tarascon, J. Electrochem. Soc. 149 (2002) A627.
[13] T.B. Massalski (Ed.), Binary Alloy Phase Diagrams, vol. 1, second ed., ASM International, 1990.
[14] M. Wachtler, M. Winter, J.O. Besenhard, J. Power Sources 105 (2002) 151.
[15] JCPDS File: 30-0097.
[16] JCPDS File: 42-1231.
[17] JCPDS File: 04-0791.
[18] JCPDS File: 04-0805.
[19] JCPDS File: 02-1097.
[20] H. Tostmann, A.J. Kropf, C.S. Johnson, J.T. Vaughey, M.M. Thackeray, Phys. Rev. B 66 (2002) 014106.